2016

Immune- and nonimmune-compartment-specific interferon responses are critical determinants of herpes simplex virus-induced generalized infections and acute liver failure

Zachary M. Parker
Geisel School of Medicine at Dartmouth

Tracy Jo Pasieka
Washington University School of Medicine in St. Louis

George A. Parker
Charles River Laboratories

David A. Leib
Geisel School of Medicine at Dartmouth

AMERICAN SOCIETY FOR MICROBIOLOGY | Journal of Virology

Immune- and Nonimmune-Compartment-Specific Interferon Responses Are Critical Determinants of Herpes Simplex Virus-Induced Generalized Infections and Acute Liver Failure

Zachary M. Parker,[a] Tracy Jo Pasieka,[b] George A. Parker,[c] David A. Leib[a]

Department of Microbiology and Immunology, Geisel School of Medicine at Dartmouth, Lebanon, New Hampshire, USA[a]; Department of Ophthalmology and Visual Sciences, Washington University School of Medicine, St. Louis, Missouri, USA[b]; Charles River Laboratories, Hillsborough, North Carolina, USA[c]

ABSTRACT

The interferon (IFN) response to viral pathogens is critical for host survival. In humans and mouse models, defects in IFN responses can result in lethal herpes simplex virus 1 (HSV-1) infections, usually from encephalitis. Although rare, HSV-1 can also cause fulminant hepatic failure, which is often fatal. Although herpes simplex encephalitis has been extensively studied, HSV-1 generalized infections and subsequent acute liver failure are less well understood. We previously demonstrated that IFN-$\alpha\beta\gamma R^{-/-}$ mice are exquisitely susceptible to liver infection following corneal infection with HSV-1. In this study, we used bone marrow chimeras of IFN-$\alpha\beta\gamma R^{-/-}$ (AG129) and wild-type (WT; 129SvEv) mice to probe the underlying IFN-dependent mechanisms that control HSV-1 pathogenesis. After infection, WT mice with either IFN-$\alpha\beta\gamma R^{-/-}$ or WT marrow exhibited comparable survival, while IFN-$\alpha\beta\gamma R^{-/-}$ mice with WT marrow had a significant survival advantage over their counterparts with IFN-$\alpha\beta\gamma R^{-/-}$ marrow. Furthermore, using bioluminescent imaging to maximize data acquisition, we showed that the transfer of IFN-competent hematopoietic cells controlled HSV-1 replication and damage in the livers of IFN-$\alpha\beta\gamma R^{-/-}$ mice. Consistent with this, the inability of IFN-$\alpha\beta\gamma R^{-/-}$ immune cells to control liver infection in IFN-$\alpha\beta\gamma R^{-/-}$ mice manifested as profoundly elevated aspartate transaminase (AST) and alanine transaminase (ALT) levels, indicative of severe liver damage. In contrast, IFN-$\alpha\beta\gamma R^{-/-}$ mice receiving WT marrow exhibited only modest elevations of AST and ALT levels. These studies indicate that IFN responsiveness of the immune system is a major determinant of viral tropism and damage during visceral HSV infections.

IMPORTANCE

Herpes simplex virus 1 (HSV-1) infection is an incurable viral infection with the most significant morbidity and mortality occurring in neonates and patients with compromised immune systems. Severe pathologies from HSV include the blindness-inducing herpetic stromal keratitis, highly debilitating and lethal herpes simplex encephalitis, and generalized infections that can lead to herpes simplex virus-induced acute liver failure. While immune compromise is a known factor, the precise mechanisms that lead to generalized HSV infections are unknown. In this study, we used and developed a mouse model system in combination with real-time bioluminescence imaging to demonstrate the relative importance of the immune and nonimmune compartments for containing viral spread and promoting host survival after corneal infection. Our results shed light on the pathogenesis of HSV infections that lead to generalized infection and acute liver failure.

Herpes simplex virus 1 (HSV-1) is an enveloped DNA virus and a member of the *Alphaherpesvirus* subfamily with high seroprevalence in the human population (1). In most cases, HSV-1 causes relatively mild orolabial cold sores, but it can cause more serious localized diseases such herpes stromal keratitis, the leading cause of infectious blindness in the United States (2, 3). Serious sequelae for HSV-1 are more common in immunocompromised hosts and neonates, with uncontrolled viral replication leading to herpes simplex encephalitis (HSE) or, more rarely, HSV sepsis leading to acute liver failure (4, 5). HSV-induced acute liver failure (ALF) is an alarmingly deadly disease with a lethality rate approaching 75% (5). The importance of studying HSV-induced ALF is underscored by the immunocompromised populations it affects, mainly patients undergoing chemotherapy, bone marrow transplant recipients, HIV patients, and women in the third trimester of pregnancy (5, 6). HSV-1 infects via the mucosae of the mouth, eyes, or genitalia, where it undergoes lytic replication in the epithelium (7). During infection of these mucosae, the virus infects innervating sensory neurons, traveling in a retrograde direction in the facial neurons back to mostly sensory ganglia, wherein HSV-1 establishes latency (8). The ability of HSV to establish latency in neurons, a nondividing cell population, hinders the ability of the immune system to fully clear the virus and renders the virus refractory to cure with antiviral treatments (9). Immune dysregulation and other stimuli cause HSV-1 to erupt from latency, traveling anterograde to the mucosal surface, where lytic replication occurs, often with shedding and infection of a new host (10).

Interferon (IFN) pathways are critical to an effective response

Received 23 July 2016 **Accepted** 14 September 2016

Accepted manuscript posted online 28 September 2016

Citation Parker ZM, Pasieka TJ, Parker GA, Leib DA. 2016. Immune- and nonimmune-compartment-specific interferon responses are critical determinants of herpes simplex virus-induced generalized infections and acute liver failure. J Virol 90:10789–10799. doi:10.1128/JVI.01473-16.

Editor: R. M. Longnecker, Northwestern University

Address correspondence to David A. Leib, david.a.leib@dartmouth.edu.

to viral infections (11, 12). Upon sensing a viral pathogen-associated molecular pattern (PAMP), activation and nuclear translocation of the transcription factors IRF3 and IRF7 lead to the expression of IFNs (13–15). Secreted IFNs act in both a paracrine and an autocrine fashion, interacting with IFN receptors on the cell surface, which then upregulates IFN-stimulated genes to induce the antiviral state (11, 12). Type I (α and β) and type II (γ) IFNs signal infected and bystander cells to upregulate the innate antiviral state and prime the adaptive response for viral clearance (12, 16). Following HSV-1 infection, humans and model hosts with defects in IFN signaling pathways are unable to control viral replication (17–19). In this scenario, encephalitis and systemic HSV-1 infections often follow, which can also lead to acute liver infection and failure (5, 20). Case reports of HSV-1-induced acute liver failure indicate that while this presentation is relatively uncommon, it has a remarkably high fatality rate, and there is very little research on this presentation of HSV-1 (5, 21, 22).

The immune factors that control HSV-1 tropism during generalized infections are largely unknown. While certain immunodeficient mice succumb rapidly to encephalitis via neurotropic HSV spread, others exhibit a more generalized viscerotropic pattern with particular involvement of the liver (23, 24). In particular, IFN-αβγR$^{-/-}$ mice succumb quickly and synchronously to HSV-1, with extremely high titers in the liver (24). Consistent with this, lacking the DNA-binding domain of Stat1, these mice essentially phenocopy IFN-αβγR$^{-/-}$ with high viral loads in the liver (24). In contrast, among mice lacking the N-terminal domain of Stat1, which exhibit a residual low-level Stat1 activity, liver infection is well controlled, and these animals succumb instead to encephalitis (24, 25). Similarly, IFN-αβR$^{-/-}$ mice exhibit only transient infection of the liver, whereas IFN-γR$^{-/-}$ mice show no liver infection (26). These findings underscore the importance of the IFN signaling pathway for control of disseminated infection. In mice and humans, a variety of mutations in the TLR3 signaling pathway (IRF-3, TYK2, MAVS, TRIF, TBK1, UNC93B1, IPS-1, and Stat1) are important for protection against HSE (19, 20, 27, 28). Other factors in the IFN pathway, such as the DNA-sensing pathway adaptor STING (23), appear to be less critical for protection from HSE following corneal infection. Together, the multitude of IFN pathway sensors and adaptors allows for temporal and metered immune responses to pathogens in a variety of tissues.

Although many components of the IFN pathway are required for protection from HSE, host factors that control generalized HSV-1 infection and hepatitis are less well understood. To begin to address these factors, we performed experiments to determine the compartment in which IFN responses were most critical for protection. In particular, we examined whether the IFN responses of infected tissues were alone protective and examined whether IFN responses of infiltrating immune cells were critical to the control of systemic infection. To examine this, we used the IFN-αβγR$^{-/-}$ mouse, which is highly sensitive to disseminated HSV-1 and a suitable model for studying viscerotropic infection (24, 29). We therefore created bone marrow chimeric mice using 129SvEv (WT) and AG129 (IFN-αβγR$^{-/-}$) strains. We utilized bioluminescent HSV strains with IVIS imaging to maximize data collection from these chimeric mice, which take many weeks to engraft and are labor-intensive to create (30–32). We show that the nonimmune tissue IFN responses of the mice were largely responsible for protection from both HSE and acute liver failure. Furthermore, in the context of susceptible IFN-αβγR$^{-/-}$ mice, the acquisition of an IFN-competent immune compartment was sufficient to control viral replication and mitigate liver disease, with little impact on HSE. Together, these data demonstrate the utility of combining bioluminescent imaging (BLI) and bone marrow chimeric mouse approaches, and show that IFN responses in the nonimmune and immune compartments play distinct roles in defining the pathogenesis of generalized HSV infections.

MATERIALS AND METHODS

Viruses, cells, and mice. Vero cells were used to propagate viruses and to determine their titers as described previously (33). The HSV-1 strain used in this study was KOS (34). The luciferase expressing KOS/Dlux/OriL strain of HSV-1 was used for BLI experiments, as previously described (31). WT (Taconic, Germantown, NY) and IFN-αβγ receptor knockout (IFN-αβγR$^{-/-}$) mice were derived from a 129SvEv background (35).

Bone marrow chimeras. Bone marrow chimeras were created by irradiating WT (CD45.2-positive) and IFN-αβγR$^{-/-}$ (CD45.1-positive) mice with two 700-Gy doses of gamma radiation with 4 h between doses. These mice were then reconstituted with 3×10^6 bone marrow cells, injected retro-orbitally. The bone marrow cells were given a minimum of 8 weeks to reconstitute the bone marrow compartment of chimeric mice. For control chimeric mice, we created WT→WT or IFN-αβγR$^{-/-}$→IFN-αβγR$^{-/-}$ chimeras reconstituted with bone marrow that matched their genotype and sex. Circulating leukocytes were analyzed by flow cytometry for CD45.1 and CD45.2, and only mice containing >85% desired chimerism were used.

Animal infection and organ harvest. All animals were housed and treated according to our approved IACUC protocol (Dartmouth protocol leib.da.1#2) and Federal regulations. Prior to corneal infection mice were anesthetized with an intraperitoneal (i.p.) injection of a mixture of ketamine (87 mg/kg) and xylazine (13 mg/kg). Corneas were scarified in a 10×10 crosshatch pattern with a 25-gauge needle and then inoculated with 2×10^6 PFU per eye in 5 μl of inoculation medium (Dulbecco modified Eagle medium [HyClone] with 2% fetal bovine serum, a final concentration of 60 U/ml penicillin [HyClone], and a final concentration of 60 μg/ml streptomycin [HyClone]) (33).

Mice were sacrificed at the specified times postinfection or once they met endpoint criteria, as defined by our approved IACUC protocol. Eye swabs were collected at the indicated time points, as previously described (36). Blood was harvested in heparin-treated tubes, and serum was separated by centrifugation at 5,000 × *g* for 5 min and then stored at −80°C. Eye swabs, spleens, livers, brains, brain stems, and trigeminal ganglia were frozen in the appropriate volume of inoculation medium at −80°C. Tissues were prepared for titering by homogenization/disruption with glass beads and sonication, as previously described (33).

Multiplex cytokine quantification. Cytokines were quantified by using a bead-based multiplex protocol as previously described (25). Serum was harvested at the days postinfection indicated and stored at −80°C until processing. Serum was diluted by an equal volume of Bio-Rad serum diluent solution (Bio-Rad, Hercules, CA). A Bradford assay was used to normalize protein levels. A BioPlex bead-based multiplex cytokine quantification kit was used according to the manufacturer's instructions (Bio-Rad). All cytokine concentrations were quantified by comparison to a standard curve. A minimum of four mice were used for each data point on each day postinfection.

Organ histology. Mice were sacrificed at the indicated days postinfection, organs harvested, and fixed in 10% neutral buffered formalin. These were then paraffin embedded, sectioned, and stained with hematoxylin and eosin by the pathology core facility at Dartmouth-Hitchcock Medical Center (Lebanon, NH). The slides were coded to conceal the treatment group and then assessed for pathology in a masked fashion.

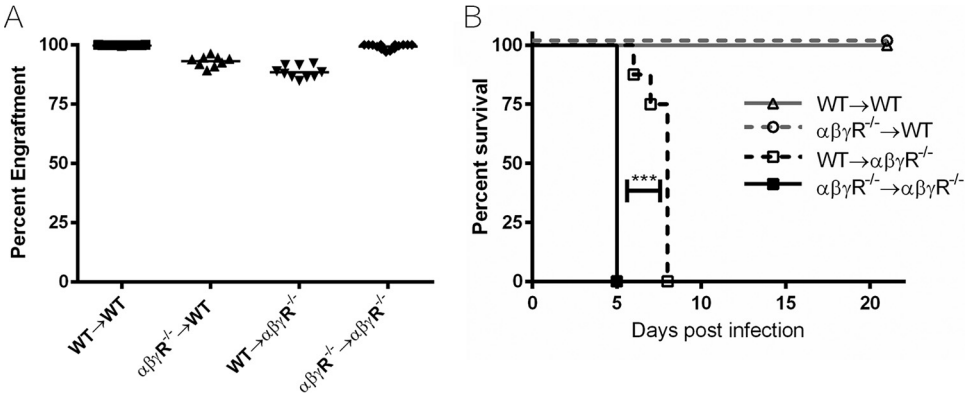

FIG 1 Percent chimerism and survival of chimeric mice following corneal infection. (A) Irradiated bone marrow recipient mice were reconstituted with desired bone marrow and confirmed using flow cytometry of CD45.1 or CD45.2 congenic markers. Mice at less than an 85% desired engraftment were not used for experiments. Data are from two representative independent chimera engraftments with ≥9 mice per group. (B) Mice were infected with 2×10^6 PFU/eye HSV-1 strain KOS and monitored for 21 days or until endpoint criteria were met. ***, $P < 0.0005$. Statistical significance was determined by a Mantel-Cox test, with two independent experiments with ≥6 mice total per group.

Bioluminescent imaging (BLI). Mice were infected corneally with KOS/Dlux/OriL and injected i.p. at the appropriate times postinfection with filter-sterilized D-luciferin potassium salt (Gold Biotech, St. Louis, MO) in phosphate-buffered saline (PBS) at 150 mg/kg. Mice were anesthetized with 2.5% isoflurane and imaged using a cooled charge-coupled device camera equipped instrument (IVIS 100; Caliper Life Sciences, Hopkinton, MA) as previously described (30). Imaging parameters (f-stop, binning, shutter speed, field of view, and scales) were all kept consistent when comparing images, as described in the figure legends. When quantifying the photon signal, the same region of interest (ROI) was placed on each mouse, and the total flux of photons per second was recorded for analysis. All images were analyzed using Igor Pro Living Image software (v2.60; Perkin-Elmer, Akron, OH).

Liver enzyme quantification. Sera were processed by centrifuging heparin-treated blood samples at 5,000 × *g* for 5 min at 4°C. Aspartate aminotransferase (AST) and alanine transaminase (ALT) were quantified on a Roche Cobas c500 analyzer (Roche Holding AG, Basel, Switzerland). ALT was quantified by using an *in vitro* test for the quantitative determination of the catalytic activity of ALT (ALTL kit; Roche). AST was quantified by using an *in vitro* test for the quantitative determination of the catalytic activity of AST (ASTL kit; Roche.

Evans blue uptake to measure blood-brain barrier (BBB) permeability. Evans blue uptake experiments were carried out as previously described (25). At 1 h prior to sacrifice, the mice were injected i.p. with 300 μl of 2% (wt/vol) Evans blue dye in PBS. Upon sacrifice, the mice were perfused with a minimum of 50 ml of PBS, and the brains were harvested into 1 ml of PBS. These samples were then homogenized with a tissue homogenizer (Omni International, Kennesaw, GA); 1 ml of 100% (wt/vol) trichloroacetic acid was added, and the samples were mixed and then incubated on ice for 30 min. The samples were centrifuged at 2,800 × *g* for 30 min at 4°C, and the supernatant optical density was quantified at 620 nm using a Bio-Rad (Hercules, CA) iMark plate reader. Increased dye concentration in the brain correlates with increased blood-brain barrier permeability.

RESULTS

The WT IFN response of immune cells confers survival advantage in IFN-αβγR$^{-/-}$ mice following HSV-1 corneal infection. Previous studies have shown that IFN-αβγR$^{-/-}$ mice quickly succumb to corneal HSV-1 infection (≤5 dpi). We sought to assess the contribution of IFN responses of the immune compartment relative to the IFN responses of the nonimmune compartment in the control of generalized infections. To accomplish this, we created IFN-αβγR$^{-/-}$ and wild-type (WT) bone marrow chimeric mice (24, 29). We generated WT mice reconstituted with WT bone marrow (WT→WT), WT with IFN-αβγR$^{-/-}$ marrow (αβγR$^{-/-}$→WT), αβγR$^{-/-}$ mice with WT marrow (WT→αβγR$^{-/-}$), or IFN-αβγR$^{-/-}$ mice reconstituted with IFN-αβγR$^{-/-}$ marrow (αβγR$^{-/-}$→αβγR$^{-/-}$) (Fig. 1A). Mice were corneally infected with 2×10^6 PFU/eye HSV-1 strain KOS and observed for 21 days postinfection (dpi) or until endpoint health criteria were met (Fig. 1B). Interestingly, the WT→αβγR$^{-/-}$ mice survived significantly longer than the αβγR$^{-/-}$→αβγR$^{-/-}$ mice, suggesting that IFN responses of bone marrow-derived cells are protective during HSV infection of IFN-defective hosts. Despite this survival advantage, both WT→αβγR$^{-/-}$ and αβγR$^{-/-}$→αβγR$^{-/-}$ mice reached endpoint criteria by ≤8 dpi. Furthermore, both WT→WT and αβγR$^{-/-}$→WT mice survived the full 21 days of the study. Together, these results suggest the IFN responses of the tissues are more critical for protection from generalized infection than IFN responses of the infiltrating immune cells from the bone marrow.

The wild-type IFN response of circulating immune cells controls viral dissemination in IFN-αβγR$^{-/-}$ mice. To examine the tropism of HSV-1 in the chimeric mice, we infected them with luciferase-expressing HSV-1 KOS/Dlux/OriL (KOSDlux) and imaged spread of the virus in using real-time BLI. The use of BLI allowed us to examine the spread of HSV in real time without the need to sacrifice mice prior to reaching the endpoint criteria, thereby extending the data obtained from these valuable chimeric mice (30, 32). Mice were infected via the cornea with KOSDlux virus at 2×10^6 PFU/eye and imaged at 3, 5, 7, and 9 dpi. In these experiments, αβγR$^{-/-}$→αβγR$^{-/-}$ mice reached the endpoint criteria at day 5, whereas WT→αβγR$^{-/-}$ mice reached the endpoint at 9 dpi due to a slight reduction in virulence of the KOSDlux virus. Although αβγR$^{-/-}$→αβγR$^{-/-}$ mice emitted an intense photon flux, mainly originating in the region of the liver at 5 dpi, the WT→αβγR$^{-/-}$ mice had significantly fewer photons emitting from the liver area at day 5 dpi, and this signal was at background levels by 9 dpi (Fig. 2A). Neither WT→WT mice nor αβγR$^{-/-}$→WT mice had disseminated virus, although the

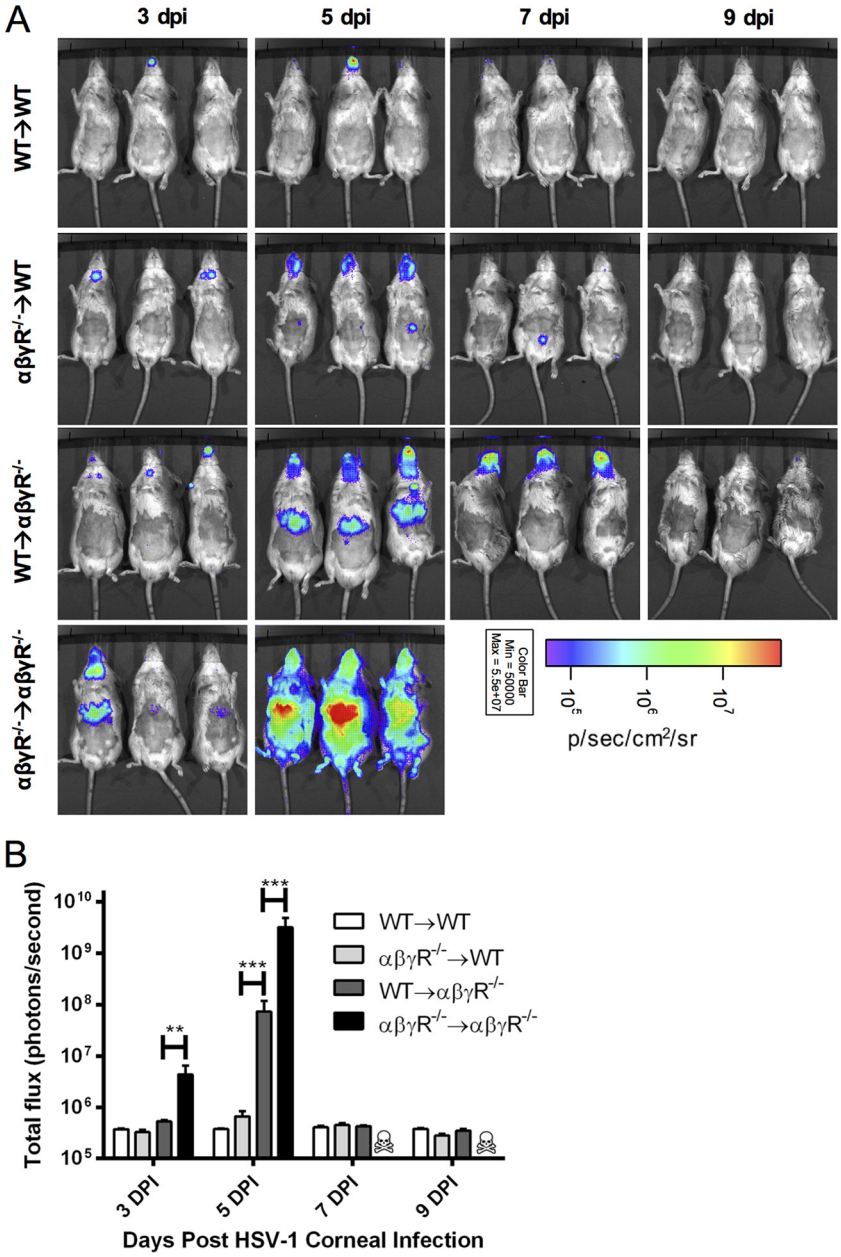

FIG 2 BLI and quantification of HSV-1 (KOSDlux) in chimeric mice following corneal infection. (A) BLI of WT→WT, $\alpha\beta\gamma R^{-/-}$→WT, WT→$\alpha\beta\gamma R^{-/-}$, and $\alpha\beta\gamma R^{-/-}$→$\alpha\beta\gamma R^{-/-}$ mice infected with 2×10^6 PFU of KOSDlux per eye. The photon flux heatmap is set to a log scale with a minimum of 5×10^4 photons (p)/s/cm^2/sr (purple) and a maximum of 5×10^7 p/s/cm^2/sr (red). (B) Total photon flux from abdomens of mice quantified using region of interest (ROI) analysis using Living Image software (Xenogen). ***, $P < 0.0005$. Statistical analysis was performed using an unpaired two-tailed *t* test. Results are from three independent experiments with ≥8 mice per group.

$\alpha\beta\gamma R^{-/-}$→WT mice demonstrated increased signal originating at the cervical lymph nodes relative to the WT→WT mice. Quantification of ventral bioluminescence was achieved through region-of-interest (ROI) analysis on the ventral abdominal area of the mice (Fig. 2B). ROI analysis revealed the highest flux from the $\alpha\beta\gamma R^{-/-}$→$\alpha\beta\gamma R^{-/-}$ mice, an observation consistent with previous data (24). Ventral bioluminescence in WT→$\alpha\beta\gamma R^{-/-}$ mice increased by 5 dpi but, surprisingly, returned to baseline levels by 7 dpi. This suggested that the virus was being controlled in the liver in these mice in an IFN-competent hematopoietic cell-dependent manner. Accordingly, both the WT→WT mice and the $\alpha\beta\gamma R^{-/-}$→WT mice had ventral bioluminescent signals at baseline throughout the experiments. To confirm which organs had the greatest bioluminescent signal at the experimental endpoints of 5 and 9 dpi, organs were harvested, and *ex vivo* BLI was performed. The signal from $\alpha\beta\gamma R^{-/-}$→$\alpha\beta\gamma R^{-/-}$ mice was saturating (Fig. 3A), and a shorter exposure was therefore performed for organs at 5 dpi to more accurately measure the very high signal from these livers (Fig. 3B). This *ex vivo* BLI showed that the highest photon flux was from the livers of

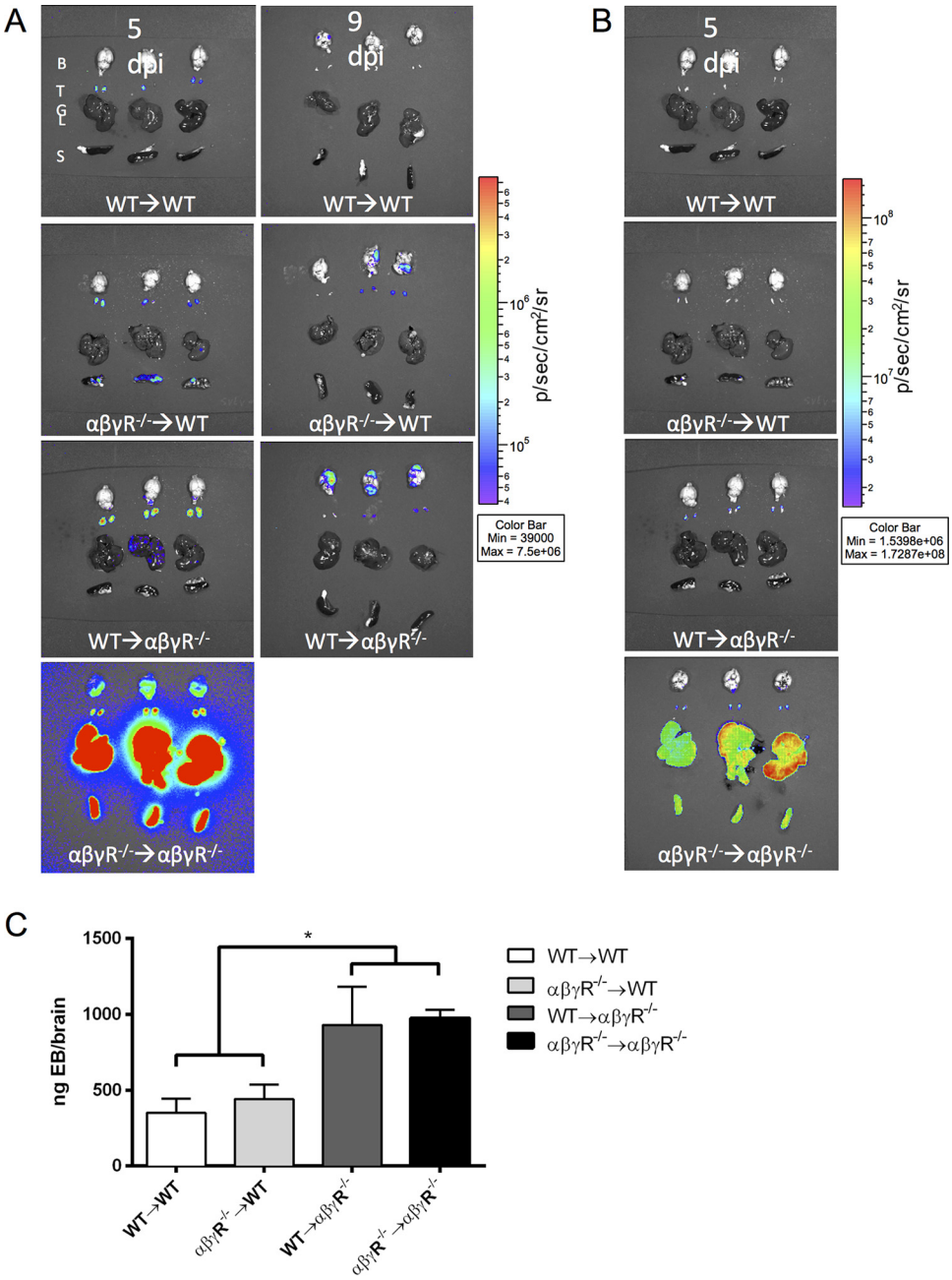

FIG 3 (A) *Ex vivo* BLI of brain (B), trigeminal ganglia (TG), liver (L), and spleen (S) of chimeric mice on terminal experimental time point (9 dpi for WT→WT, $\alpha\beta\gamma R^{-/-}$→WT, WT→$\alpha\beta\gamma R^{-/-}$, and 5 dpi for $\alpha\beta\gamma R^{-/-}$→$\alpha\beta\gamma R^{-/-}$). The photon flux heatmap is set to a log scale with a minimum of 3.9×10^4 photons (p)/s/cm^2/sr (purple) and a maximum of 7.5×10^6 p/s/cm^2/sr (red). (B) The same *ex vivo* organs from panel A at 5 dpi, but the luminescence was acquired using a shorter exposure and the image heatmap scale has a minimum of 1.54×10^6 p/s/cm^2/sr (purple) and a maximum of 1.73×10^8 p/s/cm^2/sr. (C) BBB permeability quantification using Evans blue after infection with HSV-1 (KOS) at 2×10^6 PFU/eye in mice at 7 dpi, except for $\alpha\beta\gamma R^{-/-}$→$\alpha\beta\gamma R^{-/-}$ mice, which were sacrificed at 5 dpi. BBB permeability was quantified using Evans blue dye absorbance from perfused mice brain homogenates. *, $P < 0.05$ (statistical analysis was performed using an unpaired two-tailed *t* test between columns). The results are from two independent experiments with ≥5 mice per group.

$\alpha\beta\gamma R^{-/-}$→$\alpha\beta\gamma R^{-/-}$ mice, with high signals also seen in the spleens and trigeminal ganglia, and a low signal from the brain stems. Little signal was seen with any of the 9-dpi mice compared to the 5-dpi $\alpha\beta\gamma R^{-/-}$→$\alpha\beta\gamma R^{-/-}$ mice. Substantial BLI was also seen in the brains and trigeminal ganglia at 9 dpi with both $\alpha\beta\gamma R^{-/-}$→WT and WT→$\alpha\beta\gamma R^{-/-}$ mice. The photon flux appeared to be greater in the brains of WT→$\alpha\beta\gamma R^{-/-}$ mice at 9 dpi, suggesting reduced viral control in these mice. Both chimeras, however, have demonstrated IFN deficiencies in either the hematopoietic or the nonhematopoietic compartment that allow greater viral replication in the brain and central nervous system (CNS).

Although both WT→αβγR$^{-/-}$ and αβγR$^{-/-}$→αβγR$^{-/-}$ mice succumbed to corneal infection with HSV-1 regardless of the IFN competence of their immune systems, the presence of WT immune cells in WT→αβγR$^{-/-}$ mice spared them from fulminant infection involving the liver. To examine this further, we injected mice with Evans blue dye, which only enters the CNS where there is a breach of the BBB, as happens often during encephalitis (25, 37). Evans blue dye was administered to the chimeric mice, and the absorbance of brain homogenates was quantified (Fig. 3C). All mice were sacrificed at 7 dpi, with the exception of IFN-αβγR$^{-/-}$ mice, which had to be sacrificed on 5 dpi since they met the endpoint criteria. As judged by Evans blue quantification, the BBB permeability of WT→WT or αβγR$^{-/-}$→WT mice was comparably low. In contrast, the BBB permeability of WT→αβγR$^{-/-}$ and αβγR$^{-/-}$→αβγR$^{-/-}$ mice was elevated to similar levels, suggesting that IFN-αβγR$^{-/-}$ brains cannot be protected by the IFN response of the immune compartment.

IFN responses of infected tissues are pivotal for control of viral replication. To further quantify the replication of HSV-1 in different tissues, we infected mice via the cornea with HSV-1 KOS at 2×10^6 PFU/eye and determined the viral titers (Fig. 4). In the eyes of αβγR$^{-/-}$→αβγR$^{-/-}$ mice, viral replication was 100-fold higher than in WT→αβγR$^{-/-}$ mice at both 3 and 5 dpi (Fig. 4A). This suggests that the IFN responses of WT infiltrating immune cells are important for the control of viral replication in the cornea (Fig. 4A). Further supporting this hypothesis, we observed higher viral titers in the eyes of αβγR$^{-/-}$→WT mice compared to WT→WT mice at 7 dpi. Furthermore, in contrast to the WT→WT mice, in which virus was undetectable in the cornea by 9 dpi, the αβγR$^{-/-}$→WT mice failed to clear virus, with $>10^4$ PFU/ml persisting therein. Viral replication was also more pronounced in the trigeminal ganglia of WT→αβγR$^{-/-}$ and αβγR$^{-/-}$→αβγR$^{-/-}$ mice compared to αβγR$^{-/-}$→WT or WT→WT mice (Fig. 4B). Virus was cleared from the ganglia of both αβγR$^{-/-}$→WT and WT→WT mice, and latency was established (Z. M. Parker and D. A. Leib, unpublished data). This suggests a lack of control of viral replication in the IFN-deficient nervous system, regardless of the immune cell IFN competence. Similar patterns were also observed in the brain stem and the brain (Fig. 4C and D). Unexpectedly, however, there was a stark contrast at 5 dpi in which viral titers were 10,000-fold higher in the livers of αβγR$^{-/-}$→αβγR$^{-/-}$ mice compared to WT→αβγR$^{-/-}$ mice (Fig. 4E). Viral titers in the spleen and serum were also highest in αβγR$^{-/-}$→αβγR$^{-/-}$ mice at 5 dpi relative to the other chimeras (Fig. 4F and G). Taken together, these findings suggest that the IFN responsiveness of immune cells is necessary for the efficient clearance of virus from most tissues. Nonetheless, the IFN responsiveness of the host tissues is capable of controlling viral replication to the extent that the host does not succumb to infection, regardless of the IFN receptor status of infiltrating immune cells.

IFN-competent circulating immune cells protect IFN-αβγR$^{-/-}$ mice from HSV-1-induced acute liver failure. Previous studies have shown that certain IFN-deficient mice (IFN-αβγR$^{-/-}$, Stat1$^{-/-}$) exhibit increased susceptibility to HSV liver infection (24, 26, 29). In the present study, we observed a reduced viral burden in the livers of WT→αβγR$^{-/-}$ mice relative to αβγR$^{-/-}$→αβγR$^{-/-}$ mice (Fig. 2 and 4E). We therefore hypothesized that the reduced viral burden resulting from these circulating WT immune cells would protect the liver from damage. We therefore quantified the levels of circulating aspartate aminotransferase (AST) and alanine transaminase (ALT), which, when elevated, are diagnostic for liver damage (Fig. 5A and B). The normal levels of AST and ALT are ~60 and ~28 IU/liter, respectively (38). In acute viral hepatitis, AST and ALT levels can rise to between 300 and 3,000 IU/liter. In cases of severe toxicity, such as acetaminophen overdose or ischemia, AST and ALT concentrations increase to levels ranging from 500 IU/liter up to 10,000 IU/liter. As expected, WT→WT and αβγR$^{-/-}$→WT mice showed no significant changes in serum AST or ALT throughout infection (Fig. 5A and B). In contrast, at 5 dpi both AST and ALT in αβγR$^{-/-}$→αβγR$^{-/-}$ mice were at the critically high levels of ~22,000 and ~12,000 IU/liter, respectively. This suggests that αβγR$^{-/-}$→αβγR$^{-/-}$ mice undergo acute liver damage by ≤5 dpi. Interestingly, WT→αβγR$^{-/-}$ mice showed peak AST and ALT levels of ~700 and ~450 IU/liter, respectively, by 7 dpi. While certainly elevated, these liver enzyme peaks are muted relative to those seen in αβγR$^{-/-}$→αβγR$^{-/-}$ mice, suggesting that the IFN responsiveness of the immune compartment protects the liver from damage.

To confirm and extend our AST/ALT studies, we performed histology examinations on the livers of infected chimeric mice (Fig. 5C to H). Mice were infected with KOS at 2×10^6 PFU/eye and sacrificed at 5 or 7 dpi. Hematoxylin-eosin-stained sections were examined in a masked fashion to assess the pathology in the livers of chimeric mice. In WT→WT mice at 7 dpi, the livers showed mild infiltration of lymphocytes and neutrophils and occasional apoptotic cells (indicated by an arrow), but these livers were relatively healthy (Fig. 5C). In αβγR$^{-/-}$→WT mice at 7 dpi there were slightly more foci of infiltrating lymphocytes and neutrophils compared to the WT→WT mice (Fig. 5D). In contrast to the relatively undamaged WT→WT and αβγR$^{-/-}$→WT livers, WT→αβγR$^{-/-}$ livers showed multifocal necrosis and greater numbers of infiltrating inflammatory cells (indicated by arrows Fig. 5E and F). There are infiltrating lymphocytes and neutrophils into an area of hepatic necrosis (Fig. 5F). The most severe liver pathology was in αβγR$^{-/-}$→αβγR$^{-/-}$ mice at 5 dpi in which extensive necrosis was observed (Fig. 5G and H). A degenerating hepatocyte with nuclear accumulations of peripheralized chromatin can also be seen (arrow in Fig. 5H), suggesting intranuclear viral replication. Overall, the pathology of these livers was consistent with BLI, titer, and AST/ALT data in this study.

IFN-αβγR$^{-/-}$ mice have delayed inflammatory immune responses. Viral infection and liver damage is often exacerbated through cytokine storm and immune dysregulation (39–41). Having shown that the IFN status of the immune compartment is critical for controlling generalized infections and liver damage, we sought to assess whether abnormal cytokine levels were an additional component in the liver disease observed in IFN-αβγR$^{-/-}$ mice. To address this, we took sera from infected WT and IFN-αβγR$^{-/-}$ mice and quantified 23 different cytokines using Bio-Plex (Fig. 6). At 1 dpi, the cytokine responses of WT mice were generally higher, especially the proinflammatory cytokines interleukin-1β (IL-1β) and tumor necrosis factor alpha (TNF-α) (Fig. 6A). By 3 dpi, however, inflammatory cytokine expression in WT mice had largely subsided (Fig. 6B). In contrast, the IFN-αβγR$^{-/-}$ mice exhibited a muted response by 1 dpi, but by 3 dpi

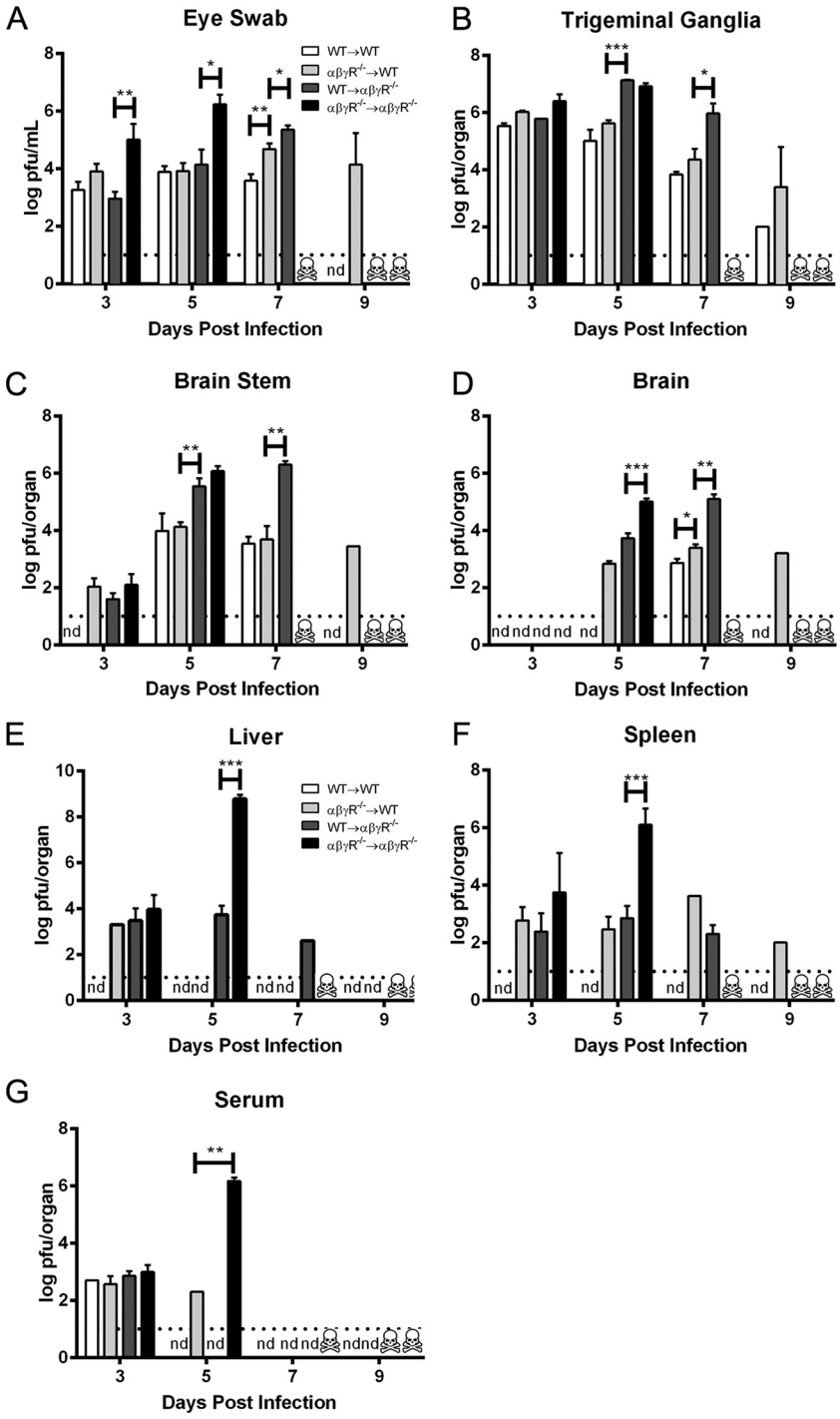

FIG 4 Viral titers in tissues of chimeric mice following corneal infection with HSV-1 (KOS) at 2×10^6 PFU/eye. Mice sacrificed on days 3, 5, 7, and 9 were used to collect titer data for eye swabs (A), trigeminal ganglia (B), brain stem (C), brain (D), liver (E), spleen (F), and serum (G). *, $P < 0.05$; **, $P < 0.005$; ***, $P < 0.0005$ (statistical significance was tested using an unpaired two-tailed *t* test). The results are from four independent experiments with ≥8 mice per group.

they showed overexpression of many cytokines, especially granulocyte colony-stimulating factor (G-CSF), TNF-α, gamma interferon (IFN-γ), and MCP-1. By 5 dpi, the cytokine levels in WT mice continued to normalize, whereas in IFN-αβγR$^{-/-}$ mice they remained persistently high, and certain cytokine levels (especially IL-6, G-CSF, and IFN-γ) continued to increase (Fig. 6C). Taken together, WT mice show a rapid, but controlled inflammatory cytokine response to infection. In contrast, IFN-αβγR$^{-/-}$ mice show a delayed cytokine response to infection which then presented as an elevated cytokine profile compared to WT mice, coincident with the IFN-αβγR$^{-/-}$ mice reaching endpoint criteria by 5 dpi.

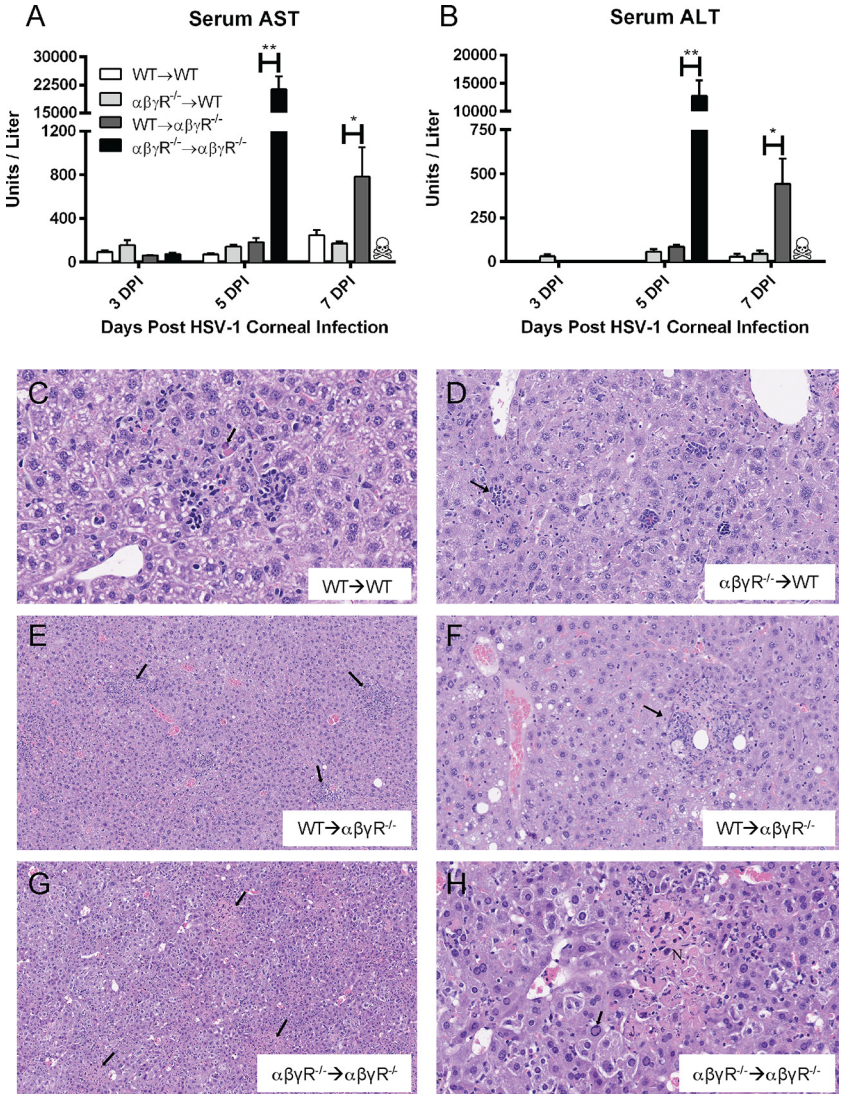

FIG 5 Serum aspartate transaminase (AST) and alanine transaminase (ALT) quantification, and liver histology after corneal infection with HSV-1 (KOS) at 2×10^6 PFU/eye. Sera from infected mice was collected at 3, 5, and 7 dpi, and then AST (A) and ALT (B) were quantified. (C to G) Hematoxylin-eosin staining of liver sections of mice at 7 dpi, except for $\alpha\beta\gamma R^{-/-} \rightarrow \alpha\beta\gamma R^{-/-}$ mice, which were sacrificed at 5 dpi when they reached endpoint criteria. (C) Liver of WT→WT mouse at 40× objective magnification. Note the mild infiltration of lymphocytes and occasional neutrophils, as well as individual apoptotic cells (arrow). (D) Liver of $\alpha\beta\gamma R^{-/-} \rightarrow$WT mouse using ×20 objective magnification. Note the multifocal infiltrates of lymphocytes with occasional neutrophils. (E and F) Liver of a $WT \rightarrow \alpha\beta\gamma R^{-/-}$ mouse at ×10 (E) and ×20 (F) objective magnifications. In panel E, note the multifocal necrosis with associated mixed inflammatory cell infiltration (arrows). Panel F is a higher-magnification view of panel E showing mixed lymphocytic and neutrophilic infiltration in an area of hepatic necrosis. Clear vacuoles in hepatocytes indicate accumulation of neutral lipid associated with metabolic disturbance. (G and H) Liver of a $\alpha\beta\gamma R^{-/-} \rightarrow \alpha\beta\gamma R^{-/-}$ mouse at ×10 (G) and ×30 (H) objective magnifications. Note the extensive multiple areas of necrosis (arrows in panel G), the large area of hepatocellular necrosis ("N" in panel H), and peripheralized chromatin (arrow in panel H), suggesting intranuclear viral replication.

DISCUSSION

HSV-1 poses a serious risk for patients who are immunocompromised, have congenital defects in the IFN and related pathways, or have underdeveloped immune responses. While there is a greater risk for these populations to experience HSE, HSV-induced acute liver failure has not been widely studied. To protect these at-risk populations, early administration of antiviral nucleoside analog drugs is key, but HSV-induced acute liver failure often goes misdiagnosed because it is relatively rare, with only ~1% of acute liver failures caused by HSV (5, 21). Although rare, HSV-induced acute liver failure has a lethality rate of near 75% (5). In the present study, we have demonstrated that the IFN responsiveness of the tissues of the host outweigh the control exerted by circulating immune cells during generalized infection with HSV-1. That said, IFN responsiveness of the circulating immune cells clearly contributes to controlling generalized infections, particularly in the liver. The incidence of HSV-induced liver failure is well established in the case report literature, with most cases occurring in immunocompromised patients, although some immunocompetent patients succumb to the disease (21, 42, 43). Although this disease has gained attention, especially in the transplant literature, to our knowledge there has been no basic research on HSV hepatotropism and the role of innate immunity therein. Most IFN pathway-deficient mice are highly susceptible to HSV-1, but most

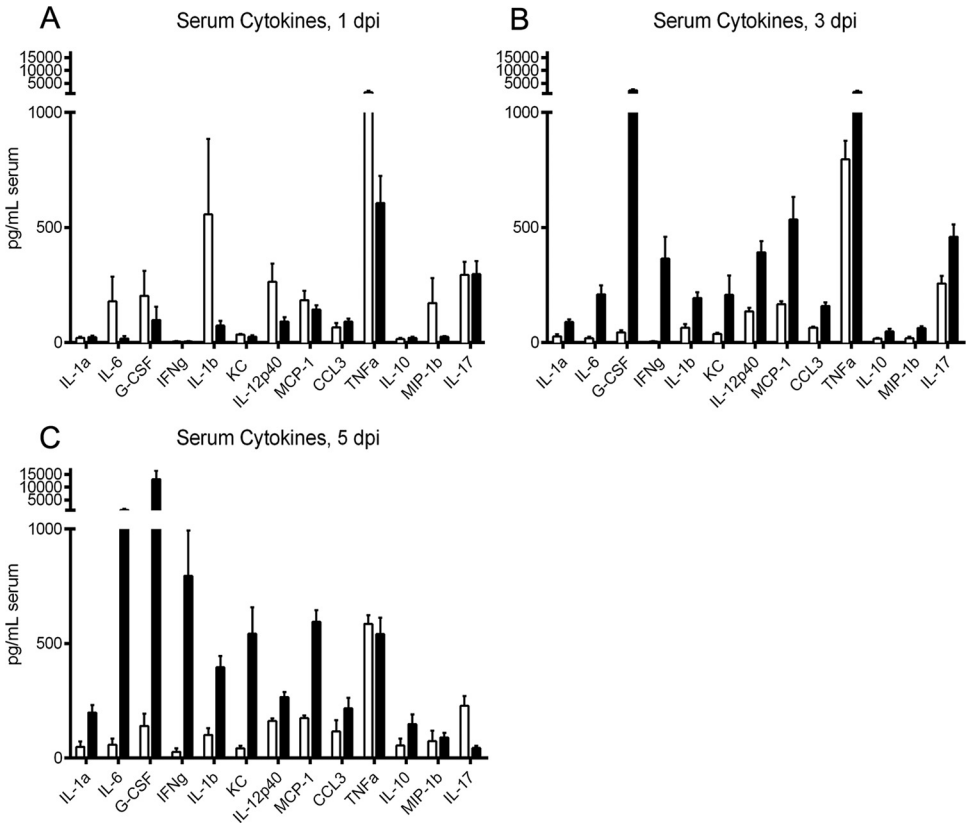

FIG 6 Serum cytokines of sera from WT and IFN-$\alpha\beta\gamma R^{-/-}$ mice measured by BioPlex following corneal infection with HSV-1 (KOS) at 2×10^6 PFU/eye. The serum cytokines from infected mice were quantified at 1 dpi (A), 3 dpi (B), and 5 dpi (C). The results are from two independent experiments with ≥10 mice per group.

of them succumb to encephalitis (44, 45). A few mouse strains (IRF3/7$^{-/-}$, Stat1 DNA-binding domain$^{-/-}$) infected with HSV exhibit pathogenesis and mortality patterns that are consistent with liver damage, although liver failure as a cause of death was not directly examined (15, 24). Interestingly, IFN-$\alpha\beta R^{-/-}$ mice show robust infection of the liver but clear the virus and survive infection, whereas IFN-γR-deficient mice show no liver infection at all (26). The results in this study are therefore consistent with synergy of type I and II IFNs when responding to generalized HSV-1 infection, in accordance with previous studies (46). Indeed, the presence of IFN-competent immune cells was sufficient to spare the mice from hepatic failure even when the nonimmune compartment was IFN deficient. It appears, therefore, that when IFN-αβγ responses are completely ablated, the mice present with severe hepatic failure upon infection with HSV-1 (15, 24).

Here, $\alpha\beta\gamma R^{-/-} \rightarrow \alpha\beta\gamma R^{-/-}$ mice had disseminated viremic disease and succumbed to acute liver failure. In contrast, WT→$\alpha\beta\gamma R^{-/-}$ mice had relatively little liver pathology, although they still showed multiple areas of necrosis at endpoint criteria. The IFN responses of the circulating immune cells in WT→$\alpha\beta\gamma R^{-/-}$ mice largely controlled viral replication in the liver, thereby reducing damage. Interestingly, this protection of the liver by IFN-competent immune cells was inadequate to fully protect the mice which reached endpoint criteria by 7 dpi. The Evans blue data suggest that the WT→$\alpha\beta\gamma R^{-/-}$ mice most likely succumb to encephalitis. The somewhat elevated AST and ALT levels in these mice may be contributing to the encephalitis readout observed (47). It appears, therefore, that in an immunocompromised host an IFN-competent immune compartment can protect the liver but not the brain. Furthermore, in WT→WT or IFN-$\alpha\beta\gamma R^{-/-}$→WT mice, survival was at 100%, and virus titers were much lower than in WT→IFN-$\alpha\beta\gamma R^{-/-}$ mice, demonstrating that the tissues and resident cells exert greater control on viral replication and survival than do circulating immune cells. It is also interesting that in the corneas of IFN-$\alpha\beta\gamma R^{-/-}$→WT mice at 9 dpi, virus was not cleared. Consistent with our data, the cornea relies on both the resident and early infiltrating immune cell response for a proper response to HSV-1 (48, 49). Our data add that the IFN competence of infiltrating immune cells is necessary for efficient viral clearance in this normally avascular site.

It should be noted that the appearance of HSV in the liver following ocular infection is not peculiar to infection of IFN-defective mice. We have observed HSV in the livers of WT mice within hours of initial infection, although this initial systemic infection is rapidly cleared (26; A. J. Charron and D. A. Leib, unpublished data). These findings, together with this study, suggest that the IFN response is irrelevant to seeding of infection in the liver. Rather, some source of IFN response is paramount for control of viral replication and liver damage, as evidenced from patterns of infection and liver disease observed in this study. That said, there is likely a role for appropriately regulated cytokine expression in the prevention of hepatic failure. Indeed, the liver is an immune privileged organ that is constantly being exposed to a variety of foreign antigens, and immune response must therefore be care-

fully regulated to avoid collateral damage (50). The liver develops a robust IFN response to liver-stage *Plasmodium* in a mouse model of infection. In this system, using either hepatocyte IFN-αβR-deficient or myeloid IFN-αβR-deficient mice, it was shown that a primary antiparasitic IFN response was driven almost exclusively by the hepatocytes, whereas the myeloid-derived IFN responses played a role later in infection (51). Our study therefore mirrors these findings in showing that IFN responses in the liver are the primary drivers of antimicrobial responses, while infiltrating immune cells play a supporting role.

Our finding of circulating cytokines in WT mice following infection shows an early inflammatory response, which is then appropriately downregulated. In IFN-$\alpha\beta\gamma R^{-/-}$ mice, however, there was a delay in the inflammatory cytokine response and then an overreaction at later days postinfection. The dysregulation seen in IFN-$\alpha\beta\gamma R^{-/-}$ mice could be either due to the incapacitated negative feedback in the IFN-dependent inflammatory pathways, or it could result from the increased PAMP signal from an increasing viral load. It is most likely that it is a combination of both factors, and the result of this dysregulated cytokine response is severe immune pathology. In either case, our study elucidated the role of compartment-specific IFN responses in virus-induced liver failure through a unique combination of BLI and bone marrow chimeric approaches. Understanding these responses and pathways will lead to more appropriate interventions in patients with HSE and HSV acute liver failure, as well as other pathogen-induced liver pathologies (5). The data presented here regarding IFN responsiveness of the liver give insight into the underlying cause of disseminated HSV infections.

ACKNOWLEDGMENTS

This study was supported by National Institutes of Health grant RO1 EY09083 to D.A.L. The project was also supported by P30RR016437 from the National Center for Research Resources to Dartmouth. Z.M.P. received training grant support from the Geisel School of Medicine Microbiology and a Molecular Pathogenesis Program Training Grant (T32AI007519 Host-Microbe Interactions).

We thank Brian North for colony maintenance and genotyping, Rendall Strawbridge for mouse irradiation, and Bill Halford for suggesting these experiments during a review of a previous paper.

FUNDING INFORMATION

This work, including the efforts of Zachary M. Parker, was funded by HHS | National Institutes of Health (NIH) (T32AI007519). This work, including the efforts of David A. Leib, was funded by HHS | National Institutes of Health (NIH) (RO1 EY09083). This work, including the efforts of David A. Leib, was funded by HHS | National Institutes of Health (NIH) (P30RR016437).

REFERENCES

1. **Xu F, Sternberg MR, Kottiri BJ, McQuillan GM, Lee FK, Nahmias AJ, Berman SM, Markowitz LE.** 2006. Trends in herpes simplex virus type 1 and type 2 seroprevalence in the United States. JAMA **296:**964–973.
2. **Barker NH.** 2008. Ocular herpes simplex. BMJ Clin Evid **2008:**pii0707.
3. **Rowe AM, St Leger AJ, Jeon S, Dhaliwal DK, Knickelbein JE, Hendricks RL.** 2013. Herpes keratitis. Prog Retinal Eye Res **32:**88–101. http://dx.doi.org/10.1016/j.preteyeres.2012.08.002.
4. **Kennedy PPGE.** 2005. Viral encephalitis. J Neurol **252:**268–272. http://dx.doi.org/10.1007/s00415-005-0770-7.
5. **Riediger C, Sauer P, Matevossian E, Müller MW, Büchler P, Friess H.** 2009. Herpes simplex virus sepsis and acute liver failure. Clin Transpl **23:**37–41. http://dx.doi.org/10.1111/j.1399-0012.2009.01108.x.
6. **Johnson JR, Egaas S, Gleaves CA, Hackman R, Bowden RA.** 1992. Hepatitis due to herpes simplex virus in marrow-transplant recipients. Clin Infect Dis **14:**38–45. http://dx.doi.org/10.1093/clinids/14.1.38.
7. **Kukhanova MK, Korovina AN, Kochetkov SN.** 2014. Human herpes simplex virus: life cycle and development of inhibitors. Biochemistry **79:**1635–1652. http://dx.doi.org/10.1134/S0006297914130124.
8. **Kennedy PGE, Rovnak J, Badani H, Cohrs RJ.** 2015. A comparison of herpes simplex virus type 1 and varicella-zoster virus latency and reactivation. J Gen Virol **96:**1581–1602. http://dx.doi.org/10.1099/vir.0.000128.
9. **Rosato PC, Leib DA.** 2015. Neurons versus herpes simplex virus: the innate immune interactions that contribute to a host–pathogen standoff. Future Virol **10:**699–714. http://dx.doi.org/10.2217/fvl.15.45.
10. **Bloom DC.** 2016. Alphaherpesvirus latency: a dynamic state of transcription and reactivation. Adv Virus Res **94:**53–80. http://dx.doi.org/10.1016/bs.aivir.2015.10.001.
11. **McNab F, Mayer-Barber K, Sher A, Wack A, O'Garra A.** 2015. Type I interferons in infectious disease. Nat Rev Immunol **15:**87–103. http://dx.doi.org/10.1038/nri3787.
12. **Bigley NJ.** 2014. Complexity of interferon-γ interactions with HSV-1. Front Immunol **5:**15.
13. **Paludan SR, Bowie AG, Horan KA, Fitzgerald KA.** 2011. Recognition of herpesviruses by the innate immune system. Nat Rev Immunol **11:**143–154. http://dx.doi.org/10.1038/nri2937.
14. **Suazo PA, Ibañez FJ, Retamal-Díaz AR, Paz-Fiblas MV, Bueno SM, Kalergis AM, González PA.** 2015. Evasion of early antiviral responses by herpes simplex viruses. Mediators Inflamm **2015:**593757. http://dx.doi.org/10.1155/2015/593757.
15. **Murphy AA, Rosato PC, Parker ZM, Khalenkov A, Leib DA.** 2013. Synergistic control of herpes simplex virus pathogenesis by IRF-3, and IRF-7 revealed through noninvasive bioluminescence imaging. Virology **444:**71–79. http://dx.doi.org/10.1016/j.virol.2013.05.034.
16. **Conrady CD, Jones H, Zheng M, Carr DJ.** 2011. A functional type I interferon pathway drives resistance to cornea herpes simplex virus type 1 infection by recruitment of leukocytes. J Biomed Res **25:**111–119. http://dx.doi.org/10.1016/S1674-8301(11)60014-6.
17. **Sancho-Shimizu V, Pérez de Diego R, Lorenzo L, Halwani R, Alangari A, Israelsson E, Fabrega S, Cardon A, Maluenda J, Tatematsu M, Mahvelati F, Herman M, Ciancanelli M, Guo Y, AlSum Z, Alkhamis N, Al-Makadma AS, Ghadiri A, Boucherit S, Plancoulaine S, Picard C, Rozenberg F, Tardieu M, Lebon P, Jouanguy E, Rezaei N, Seya T, Matsumoto M, Chaussabel D, Puel A, Zhang S-Y, Abel L, Al-Muhsen S, Casanova J-L.** 2011. Herpes simplex encephalitis in children with autosomal recessive and dominant TRIF deficiency. J Clin Invest **121:**4889–4902. http://dx.doi.org/10.1172/JCI59259.
18. **Lim HK, Seppänen M, Hautala T, Ciancanelli MJ, Itan Y, Lafaille FG, Dell W, Lorenzo L, Byun M, Pauwels E, Rönnelid Y, Cai X, Boucherit S, Jouanguy E, Paetau A, Lebon P, Rozenberg F, Tardieu M, Abel L, Yildiran A, Vergison A, Roivainen R, Etzioni A, Tienari PJ, Casanova J-L, Zhang S-Y.** 2014. TLR3 deficiency in herpes simplex encephalitis: high allelic heterogeneity and recurrence risk. Neurology **83:**1888–1897. http://dx.doi.org/10.1212/WNL.0000000000000999.
19. **Zhang S-Y, Jouanguy E, Ugolini S, Smahi A, Elain G, Romero P, Segal D, Sancho-Shimizu V, Lorenzo L, Puel A, Picard C, Chapgier A, Plancoulaine S, Titeux M, Cognet C, von Bernuth H, Ku C-L, Casrouge A, Zhang X-X, Barreiro L, Leonard J, Hamilton C, Lebon P, Héron B, Vallée L, Quintana-Murci L, Hovnanian A, Rozenberg F, Vivier E, Geissmann F, Tardieu M, Abel L, Casanova J-L.** 2007. TLR3 deficiency in patients with herpes simplex encephalitis. Science **317:**1522–1527. http://dx.doi.org/10.1126/science.1139522.
20. **Sancho-Shimizu V, Perez de Diego R, Jouanguy E, Zhang S-Y, Casanova J-L.** 2011. Inborn errors of anti-viral interferon immunity in humans. Curr Opin Virol **1:**487–496. http://dx.doi.org/10.1016/j.coviro.2011.10.016.
21. **Norvell JP, Blei AT, Jovanovic BD, Levitsky J.** 2007. Herpes simplex virus hepatitis: an analysis of the published literature and institutional cases. Liver Transpl **13:**1428–1434. http://dx.doi.org/10.1002/lt.21250.
22. **McGoogan KE, Haafiz AB, González Peralta RP.** 2011. Herpes simplex virus hepatitis in infants: clinical outcomes and correlates of disease severity. J Pediatr **159:**608–611. http://dx.doi.org/10.1016/j.jpeds.2011.03.017.
23. **Parker ZM, Murphy AA, Leib DA.** 2015. Role of the DNA sensor STING in protection from lethal infection following corneal and intracerebral challenge with herpes simplex virus 1. J Virol **89:**11080–11091. http://dx.doi.org/10.1128/JVI.00954-15.
24. **Pasieka TJ, Collins L, O'Connor MA, Chen Y, Parker ZM, Berwin BL,**

Piwnica-Worms DR, Leib DA. 2011. Bioluminescent imaging reveals divergent viral pathogenesis in two strains of Stat1-deficient mice, and in αβγ interferon receptor-deficient mice. PLoS One **6:**e24018. http://dx.doi.org/10.1371/journal.pone.0024018.

25. **Pasieka TJ, Cilloniz C, Carter VS, Rosato P, Katze MG, Leib DA.** 2011. Functional genomics reveals an essential and specific role for Stat1 in protection of the central nervous system following herpes simplex virus corneal infection. J Virol **85:**12972–12981. http://dx.doi.org/10.1128/JVI.06032-11.
26. **Luker GD, Prior JL, Song J, Pica CM, Leib DA.** 2003. Bioluminescence imaging reveals systemic dissemination of herpes simplex virus type 1 in the absence of interferon receptors. J Virol **77:**11082–11093. http://dx.doi.org/10.1128/JVI.77.20.11082-11093.2003.
27. **Menasria R, Boivin N, Lebel M, Piret J, Gosselin J, Boivin G.** 2013. Both TRIF and IPS-1 adaptor proteins contribute to the cerebral innate immune response against herpes simplex virus 1 infection. J Virol **87:**7301–7308. http://dx.doi.org/10.1128/JVI.00591-13.
28. **Mørk N, Kofod-Olsen E, Sørensen KB, Bach E, zxzxswslzxzxOrntoft TF, zxzxswslzxzxOstergaard L, Paludan SR, Christiansen M, Mogensen TH.** 2015. Mutations in the TLR3 signaling pathway and beyond in adult patients with herpes simplex encephalitis. Genes Immun **16:**552–566. http://dx.doi.org/10.1038/gene.2015.46.
29. **Pasieka TJ, Menachery VD, Rosato PC, Leib DA.** 2012. Corneal replication is an interferon response-independent bottleneck for virulence of herpes simplex virus 1 in the absence of virion host shutoff. J Virol **86:**7692–7695. http://dx.doi.org/10.1128/JVI.00761-12.
30. **Luker GD, Bardill JP, Prior JL, Pica CM, Piwnica-Worms D, Leib DA.** 2002. Noninvasive bioluminescence imaging of herpes simplex virus type 1 infection and therapy in living mice. J Virol **76:**12149–12161. http://dx.doi.org/10.1128/JVI.76.23.12149-12161.2002.
31. **Summers BC, Leib DA.** 2002. Herpes simplex virus type 1 origins of DNA replication play no role in the regulation of flanking promoters. J Virol **76:**7020–7029. http://dx.doi.org/10.1128/JVI.76.14.7020-7029.2002.
32. **Luker GD, Leib DA.** 2005. Luciferase real-time bioluminescence imaging for the study of viral pathogenesis. Methods Mol Biol **292:**285–296.
33. **Rader KA, Ackland-Berglund CE, Miller JK, Pepose JS, Leib DA.** 1993. In vivo characterization of site-directed mutations in the promoter of the herpes simplex virus type 1 latency-associated transcripts. J Gen Virol **74:**1859–1869. http://dx.doi.org/10.1099/0022-1317-74-9-1859.
34. **Smith KO.** 1964. Relationship between the envelope and the infectivity of herpes simplex virus. Proc Soc Exp Biol Med **115:**814–816. http://dx.doi.org/10.3181/00379727-115-29045.
35. **van den Broek MF, Müller U, Huang S, Aguet M, Zinkernagel RM.** 1995. Antiviral defense in mice lacking both alpha/beta and gamma interferon receptors. J Virol **69:**4792–4796.
36. **Leib DA, Coen DM, Bogard CL, Hicks KA, Yager DR, Knipe DM, Tyler KL, Schaffer PA.** 1989. Immediate-early regulatory gene mutants define different stages in the establishment and reactivation of herpes simplex virus latency. J Virol **63:**759–768.
37. **Zhou J, Stohlman SA, Hinton DR, Marten NW.** 2003. Neutrophils promote mononuclear cell infiltration during viral-induced encephalitis. J Immunol **170:**3331–3336. http://dx.doi.org/10.4049/jimmunol.170.6.3331.
38. **Fernández I, Peña A, Teso ND, Pérez V, Rodríguez-Cuesta J.** 2010. Clinical biochemistry parameters in C57BL/6J mice after blood collection from the submandibular vein and retroorbital plexus. J Am Assoc Lab Anim Sci **49:**202–206.
39. **Brisse E, Imbrechts M, Put K, Avau A, Mitera T, Berghmans N, Rutgeerts O, Waer M, Ninivaggi M, Kelchtermans H, Boon L, Snoeck R, Wouters CH, Andrei G, Matthys P.** 2016. Mouse cytomegalovirus infection in BALB/c mice resembles virus-associated secondary hemophagocytic lymphohistiocytosis and shows a pathogenesis distinct from primary hemophagocytic lymphohistiocytosis. J Immunol **196:**3124–3134. http://dx.doi.org/10.4049/jimmunol.1501035.
40. **Phanthanawiboon S, Limkittikul K, Sakai Y, Takakura N, Saijo M, Kurosu T.** 2016. Acute systemic infection with dengue virus leads to vascular leakage and death through tumor necrosis factor-α and Tie2/angiopoietin signaling in mice lacking type I and II interferon receptors. PLoS One **11:**e0148564. http://dx.doi.org/10.1371/journal.pone.0148564.
41. **Oh IS, Park S-H.** 2015. Immune-mediated liver injury in hepatitis B virus infection. Immune Netw **15:**191–198. http://dx.doi.org/10.4110/in.2015.15.4.191.
42. **Poley RA, Snowdon JF, Howes DW.** 2011. Herpes simplex virus hepatitis in an immunocompetent adult: a fatal outcome due to liver failure. Case Rep Crit Care **2011:**138341.
43. **Al Midani A, Pinney J, Field N, Atkinson C, Haque T, Harber M.** 2011. Fulminant hepatitis following primary herpes simplex virus infection. Saudi J Kidney Dis Transpl **22:**107–111.
44. **Meraz MA, White JM, Sheehan KC, Bach EA, Rodig SJ, Dighe AS, Kaplan DH, Riley JK, Greenlund AC, Campbell D, Carver-Moore K, DuBois RN, Clark R, Aguet M, Schreiber RD.** 1996. Targeted disruption of the Stat1 gene in mice reveals unexpected physiologic specificity in the JAK-STAT signaling pathway. Cell **84:**431–442. http://dx.doi.org/10.1016/S0092-8674(00)81288-X.
45. **Menachery VD, Pasieka TJ, Leib DA.** 2010. Interferon regulatory factor 3-dependent pathways are critical for control of herpes simplex virus type 1 central nervous system infection. J Virol **84:**9685–9694. http://dx.doi.org/10.1128/JVI.00706-10.
46. **Sainz B, Halford WP.** 2002. Alpha/beta interferon and gamma interferon synergize to inhibit the replication of herpes simplex virus type 1. J Virol **76:**11541–11550. http://dx.doi.org/10.1128/JVI.76.22.11541-11550.2002.
47. **Nguyen JH.** 2012. Blood-brain barrier in acute liver failure. Neurochem Int **60:**676–683. http://dx.doi.org/10.1016/j.neuint.2011.10.012.
48. **Buela K-AG, Hendricks RL.** 2015. Cornea-infiltrating and lymph node dendritic cells contribute to $CD4^+$ T cell expansion after herpes simplex virus-1 ocular infection. J Immunol **194:**379–387. http://dx.doi.org/10.4049/jimmunol.1402326.
49. **Frank GM, Buela K-AG, Maker DM, Harvey SAK, Hendricks RL.** 2012. Early responding dendritic cells direct the local NK response to control herpes simplex virus 1 infection within the cornea. J Immunol **188:**1350–1359. http://dx.doi.org/10.4049/jimmunol.1101968.
50. **Horst AK, Neumann K, Diehl L, Tiegs G.** 2016. Modulation of liver tolerance by conventional and nonconventional antigen-presenting cells and regulatory immune cells. Cell Mol Immunol **13:**277–292. http://dx.doi.org/10.1038/cmi.2015.112.
51. **Liehl P, Zuzarte-Luís V, Chan J, Zillinger T, Baptista F, Carapau D, Konert M, Hanson KK, Carret C, Lassnig C, Müller M, Kalinke U, Saeed M, Chora AF, Golenbock DT, Strobl B, Prudêncio M, Coelho LP, Kappe SH, Superti-Furga G, Pichlmair A, Vigário AM, Rice CM, Fitzgerald KA, Barchet W, Mota MM.** 2014. Host-cell sensors for *Plasmodium* activate innate immunity against liver-stage infection. Nat Med **20:**47–53. http://dx.doi.org/10.1038/nm.3424.